Fig. S3. Influence of VIII-2236 on the APTT-shortening activity of rpoFVIII, ACE910 or rhFVIII in human FVIII-deficient plasma. In the absence of VIII-2236, rpoFVIII, ACE910 and rhFVIII concentration-dependently shortened the APTT of human FVIII-deficient plasma.

Fig. S4. Pharmacodynamic study and multiple dosing simulations of rpoFVIII in cynomolgus monkeys.

References

1 Den Uijl IE, Fischer K, van der Bom JG, Grobbee DE, Rosendaal FR, Plug I. Clinical outcome of moderate haemophilia compared with severe and mild haemophilia. *Haemophilia* 2009; **15**: 83–90.

2 Berntorp E, Shapiro AD. Modern haemophilia care. *Lancet* 2012; **379**: 1447–56.

3 Astermark J, Donfield SM, DiMichele DM, Gringeri A, Gilbert SA, Waters J, Berntorp E. A randomized comparison of bypassing agents in hemophilia complicated by an inhibitor: the FEIBA NovoSeven Comparative (FENOC) Study. *Blood* 2007; **109**: 546–51.

4 Hay CR, DiMichele DM. The principal results of the International Immune Tolerance Study: a randomized dose comparison. *Blood* 2012; **119**: 1335–44.

5 Manco-Johnson MJ, Abshire TC, Shapiro AD, Riske B, Hacker MR, Kilcoyne R, Ingram JD, Manco-Johnson ML, Funk S, Jacobson L, Valentino LA, Hoots WK, Buchanan GR, DiMichele D, Recht M, Brown D, Leissinger C, Bleak S, Cohen A, Mathew P. Prophylaxis versus episodic treatment to prevent joint disease in boys with severe hemophilia. *N Engl J Med* 2007; **357**: 535–44.

6 Oldenburg J. Prophylaxis in bleeding disorders. *Thromb Res* 2011; **127**: S14–17.

7 Ragni M, Fogarty P, Josephson N, Neff A, Raffini L, Kessler C. Survey of current prophylaxis practices and bleeding characteristics of children with severe haemophilia A in US haemophilia treatment centres. *Haemophilia* 2012; **18**: 63–8.

8 Kitazawa T, Igawa T, Sampei Z, Muto A, Kojima T, Soeda T, Yoshihashi K, Okuyama-Nishida Y, Saito H, Tsunoda H, Suzuki T, Adachi H, Miyazaki T, Ishii S, Kamata-Sakurai M, Iida T, Harada A, Esaki K, Funaki M, Moriyama C. A bispecific antibody to factors IXa and X restores factor VIII hemostatic activity in a hemophilia A model. *Nat Med* 2012; **18**: 1570–4.

9 Sampei Z, Igawa T, Soeda T, Okuyama-Nishida Y, Moriyama C, Wakabayashi T, Tanaka E, Muto A, Kojima T, Kitazawa T, Yoshihashi K, Harada A, Funaki M, Haraya K, Tachibana T, Suzuki S, Esaki K, Nabuchi Y, Hattori K. Identification and multidimensional optimization of an asymmetric bispecific IgG antibody mimicking the function of factor VIII cofactor activity. *PLoS ONE* 2013; **8**: e57479.

10 Den Uijl IE, Mauser Bunschoten EP, Roosendaal G, Schutgens RE, Biesma DH, Grobbee DE, Fischer K. Clinical severity of haemophilia A: does the classification of the 1950s still stand? *Haemophilia* 2011; **17**: 849–53.

11 Shima M, Matsumoto T, Ogiwara K. New assays for monitoring haemophilia treatment. *Haemophilia* 2008; **14**: 83–92.

12 Srivastava A, Brewer AK, Mauser-Bunschoten EP, Key NS, Kitchen S, Llinas A, Ludlam CA, Mahlangu JN, Mulder K, Poon MC, Street A. Guidelines for the management of hemophilia. *Haemophilia* 2013; **19**: e1–47.

13 Lillicrap D. The future of hemostasis management. *Pediatr Blood Cancer* 2013; **60**: S44–7.

14 Pipe SW. The hope and reality of long-acting hemophilia products. *Am J Hematol* 2012; **87**: S33–9.

15 Collins PW. Personalized prophylaxis. *Haemophilia* 2012; **18**: 131–5.

16 Deng R, Iyer S, Theil FP, Mortensen DL, Fielder PJ, Prabhu S. Projecting human pharmacokinetics of therapeutic antibodies from nonclinical data: what have we learned? *MAbs* 2011; **3**: 61–6.

17 Dong J, Salinger D, Endres C, Gibbs J, Hsu C, Stouch B, Hurh E, Gibbs M. Quantitative prediction of human pharmacokinetics for monoclonal antibodies: retrospective analysis of monkey as a single species for first-in-human prediction. *Clin Pharmacokinet* 2011; **50**: 131–42.

18 Ponce R, Abad L, Amaravadi L, Gelzleichter T, Gore E, Green J, Gupta S, Herzyk D, Hurst C, Ivens IA, Kawabata T, Maier C, Mounho B, Rup B, Shankar G, Smith H, Thomas P, Wierda D. Immunogenicity of biologically-derived therapeutics: assessment and interpretation of nonclinical safety studies. *Regul Toxicol Pharmacol* 2009; **54**: 164–82.

19 Igawa T, Tsunoda H, Kuramochi T, Sampei Z, Ishii S, Hattori K. Engineering the variable region of therapeutic IgG antibodies. *MAbs* 2011; **3**: 243–52.

Molecular Immunology 58 (2014) 132–138

Contents lists available at ScienceDirect

Molecular Immunology

journal homepage: www.elsevier.com/locate/molimm

Crystal structure of a novel asymmetrically engineered Fc variant with improved affinity for FcγRs

F. Mimoto, S. Kadono, H. Katada, T. Igawa*, T. Kamikawa, K. Hattori

Research Division, Chugai Pharmaceutical Co., Ltd., Japan

ARTICLE INFO

Article history:
Received 26 August 2013
Received in revised form
20 November 2013
Accepted 23 November 2013
Available online 14 December 2013

Keywords:
ADCC
Effector function
X-ray structure
FcγR interactions
Fc engineering

ABSTRACT

Enhancing the effector function by optimizing the interaction between Fc and Fcγ receptor (FcγR) is a promising approach to enhance the potency of anticancer monoclonal antibodies (mAbs). To date, a variety of Fc engineering approaches to modulate the interaction have been reported, such as afucosylation in the heavy chain Fc region or symmetrically introducing amino acid substitutions into the region, and there is still room to improve FcγR binding and thermal stability of the C_H2 domain with these approaches. Recently, we have reported that asymmetric Fc engineering, which introduces different substitutions into each Fc region of heavy chain, can further improve the FcγR binding while maintaining the thermal stability of the C_H2 domain by fine-tuning the asymmetric interface between the Fc domain and FcγR. However, the structural mechanism by which the asymmetrically engineered Fc improved FcγR binding remained unclear. In order to elucidate the mechanism, we solved the crystal structure of a novel asymmetrically engineered Fc, asym-mAb23, in complex with FcγRIIIa. Asym-mAb23 has enhanced binding affinity for both FcγRIIIa and FcγRIIa at the highest level of previously reported Fc variants. The structural analysis reveals the features of the asymmetrically engineered Fc in comparison with symmetric Fc and how each asymmetrically introduced substitution contributes to the improved interaction between asym-mAb23 and FcγRIIIa. This crystal structure could be utilized to enable us to design a more potent asymmetric Fc.

1. Introduction

Effector functions including antibody-dependent cell-mediated cytotoxicity (ADCC) and antibody-dependent cell-mediated phagocytosis (ADCP) significantly contribute to the efficacy and potency of anticancer therapeutic monoclonal antibodies (mAbs) (Scott et al., 2012). According to cumulative evidence, the potency of the antibodies can be enhanced by improving the binding affinity for Fcγ receptors (FcγRs), which are expressed on effector cells such as NK cells and macrophages (Scott et al., 2012). There have been a number of reports about engineering the heavy chain Fc region to improve the binding affinity for FcγRs by methods such as afucosylation of the N-linked glycan attached to Asn297 (Shields et al., 2002; Shinkawa et al., 2003) or symmetrically introducing amino acid substitutions into the heavy chain Fc region with or without the N-linked glycan attached to Asn297 (Green et al., 2002; Jung et al., 2010; Lazar et al., 2006; Richards et al., 2008; Sazinsky et al., 2008; Stavenhagen et al., 2007). These engineered Fc variants enhanced the binding affinity for FcγRIIa and FcγRIIIa or improved the ratio of activating FcγR binding to inhibitory FcγR binding (A/I ratio), which resulted in enhanced ADCP and ADCC activity. However, these symmetric Fc engineering approaches cannot achieve a high affinity for both FcγRIIIa high- and low-affinity allotypes and improve the A/I ratio and maintain thermal stability of the C_H2 domain at the same time. Recently, we have reported a novel potent Fc variant that maximized the effector function by an asymmetric Fc engineering approach (Mimoto et al., 2013). We introduced different amino acid substitutions into each heavy chain Fc region in an asymmetric manner to optimize the asymmetric interface between the Fc region and FcγR to successfully design an asymmetric Fc variant that had the highest affinity for both FcγRIIIa high- and low-affinity allotypes, had superior or at least comparable ADCC with the previously reported symmetrically engineered antibody, and had the

Abbreviations: ADCC, antibody-dependent cell-mediated cytotoxicity; ADCP, antibody-dependent cell-mediated phagocytosis; A/I ratio, activating FcγR binding to inhibitory FcγR binding; asym-mAb23, a novel asymmetrically engineered Fc; FcγR, Fcγ receptor; mAb, monoclonal antibody; PDB, Protein Data Bank; PBMC, peripheral blood mononuclear cells; rms, root-mean-square; SPR, surface plasmon resonance.

* Corresponding author at: 1-135 Komakado, Gotemba, Shizuoka, Japan. Tel.: +81 550 87 6734; fax: +81 550 87 5326.
E-mail address: igawatmy@chugai-pharm.co.jp (T. Igawa).

0161-5890
http://dx.doi.org/10.1016/j.molimm.2013.11.017

highest A/I ratio. However, the mechanism by which the asymmetrically introduced substitutions contribute to the improved FcγR binding remained unclear.

Here we report a crystal structure of the novel asymmetrically engineered Fc variant, asym-mAb23, in complex with FcγRIIIa. In contrast to the previously reported asymmetrically engineered Fc variant (Mimoto et al., 2013), asym-mAb23 enhanced the binding affinity for both FcγRIIIa and FcγRIIa to a level comparable with that of previously reported Fc variants for both FcγRIIIa (Lazar et al., 2006) and FcγRIIa (Richards et al., 2008). This is the first report describing the structure of asymmetrically engineered Fc variant with increased affinity for FcγRs. This crystal structure sheds light on the molecular mechanisms behind the interaction between FcγRs and asymmetrically engineered Fc variant, which will be beneficial for further designing a more potent asymmetric Fc variant.

2. Materials and methods

2.1. Preparation of antibodies and FcγRs

The antibody variants used in the experiments were expressed transiently in FreeStyle™ 293 cells (Life Technologies) transfected with plasmids encoding heavy and light chains and purified from culture supernatants using rProtein A Sepharose 4 Fast Flow or rProtein G Sepharose 4 Fast Flow (GE Healthcare), as previously described (Mimoto et al., 2013). Asymmetrically engineered Fc variants contained knobs-into-holes substitutions, Y349C/T366W in one of the heavy chains and D356C/T366S/L368A/Y407V in the other, to facilitate heterodimerization (Klein et al., 2012).

The FcγRs used in the experiments were also expressed transiently in FreeStyle™ 293 cells (Life Technologies), as previously described (Mimoto et al., 2013).

2.2. Surface plasmon resonance (SPR) analysis

The kinetic analysis of antibody variants for human FcγRs was monitored by SPR analysis using a Biacore 4000 instrument (GE Healthcare), as previously described (Mimoto et al., 2013). A recombinant protein A/G (Thermo Scientific) was immobilized on a CM5 sensor chip (GE Healthcare) using a standard primary amine-coupling protocol. HBS-EP+ (GE Healthcare) was used as the running buffer. Antibody variants were captured on the chip, followed by injection of FcγRs. The assay concentrations are from 0.001 nM to 16 nM for FcγRI, from 0.49 nM to 2000 nM for FcγRIIa, from 2.0 nM to 8000 nM for FcγRIIb, and from 0.12 nM to 2000 nM for FcγRIIIa. The experiments were conducted independently, in triplicate.

2.3. ADCC assay

Cytotoxicity of antibody against antigen A was measured using a standard calcein-AM release assay, as previously described (Mimoto et al., 2013). We used DLD-1 cells expressing tumor antigen A as target cells for the assay. Peripheral blood mononuclear cells (PBMC) were purified from whole human blood of healthy donors and used as effector cells. Antibody solution was mixed with the target cells (1×10^4 cells) and then the effector cells were added to the solution at a ratio of 50:1 PBMC to target cells.

2.4. Preparation of Fc fragments and FcγRIIIa for crystallization

We cloned a recombinant Fc fragment of asym-mAb23, Fc (asym-mAb23), corresponding to the heavy chain residues from 216 (EU numbering) to C-terminus for the crystallization. Cys220 was replaced with Ser so that the free cysteine would not make disulfide bonds. FcγRIIIa with N35Q, N71Q, and N166Q substitutions was prepared as previously described (Ferrara et al., 2011). The complex of Fc (asym-mAb23) and FcγRIIIa was prepared by mixing the Fc fragment with a little excess of FcγRIIIa, and purified by size exclusion chromatography.

Table 1
Data collection and refinement statistics.

	Fc (asym-mAb23)-FcγRIIIa
Data collection	
Space group	$P2_1$
Cell dimensions	
a, *b*, *c* (Å)	75.03, 72.49, 163.48
α, *β*, *γ* (°)	90, 91.15, 90
Resolution (Å)	2.78 (2.85–2.78)[a]
Rsym	0.078 (0.614)
I/σI	13.9 (2.1)
Completeness (%)	98.1 (98.2)
Redundancy	3.8 (3.4)
Refinement	
Resolution (Å)	25–2.78
No. reflections	41,404
Rwork/Rfree	23.6/27.4
No. atoms	9961
Average *B* factors	54.7
rms deviations	
Bond lengths (Å)	0.005
Bond angles (°)	0.962
Ramachandran statistics	
Most favored (%)	96.4
Additional allowed (%)	3.3
Disallowed (%)	0.3

Number of crystals for each structure is one.
[a] Values in parentheses are for highest-resolution shell.

2.5. Crystallization

Diffraction-quality crystals were obtained by 1:1 mixing of the 10 mg/ml protein complex of Fc (asym-mAb23) and FcγRIIIa with 0.1 M Bis–Tris pH 6.25, 0.2 M sodium iodide, and 14.5% PEG 3350 in hanging drop vapor diffusion setups with streak seeding at 20 °C.

2.6. Data collection

For data collection, crystals were flash frozen at 95 K in precipitant solution containing 20% ethylene glycol. Diffraction data to 2.78 Å were collected using the Photon Factory beamline BL-NE3A. Data were processed with Xia2 (Winter, 2010), XDS Package (Kabsch, 2010), and Scala (Evans, 2006).

2.7. Structure determination

The crystals belong to the space group $P2_1$ with cell parameters of $a = 75.03$ Å, $b = 72.49$ Å, $c = 163.48$ Å, and $\beta = 91.15°$. The structure was determined by molecular replacement with PHASER (McCoy et al., 2007) using the structure of IgG1-Fc fragment, Fc (IgG1), and FcγRIIIa complex (PDB: 3SGJ) as a search model. The asymmetric unit contains two 1:1 complexes of Fc (asym-mAb23) and FcγRIIIa. A model was built with the program Coot (Emsley et al., 2010) and refined with the program REFMAC5 (Murshudov et al., 2011). Data collection and refinement statistics are summarized in Table 1. When numbering, the standard EU numbering was used for the heavy chain Fc region. For FcγRIIIa, the FcγRII numbering system was used like PDB entry 1E4K (Sondermann et al., 2000). To convert to standard NCBI numbering, it is necessary to add three to the amino acid residue number of FcγRIIIa. All graphical presentations were prepared with PyMOL (DeLano, 2002). Superposition and calculation of root-mean-square (rms) differences were done by LSQKAB (Kabsch, 1976) in CCP4 program suite. Coordinates and

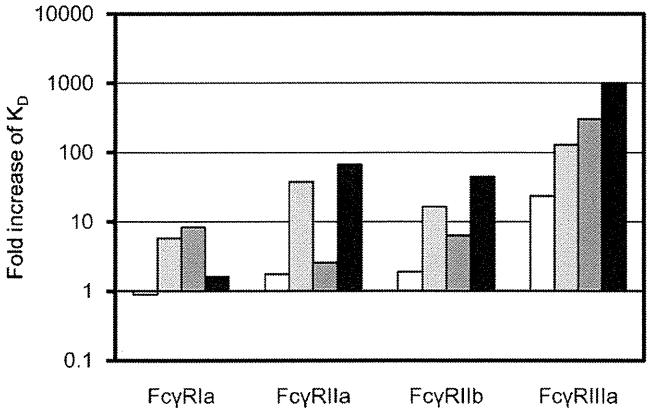

Fig. 1. Affinity analysis of antibody Fc variants for FcγRs by SPR. Fold increase of the binding affinity for each FcγR was calculated by the equation, K_D (control)/K_D (Fc variants). As the control, the K_D value of IgG1 is used for afucosyl mAb and the K_D value of IgG1 with knobs-into-holes substitutions is used for ADE variant, DLE variant, and asym-mAb23. The K_D used for the calculation is the mean value of the triplicate independent experiments. Bar colors are as follows: white, afucosyl mAb; light gray, ADE variant; dark gray, DLE variant; and black, asym-mAb23.

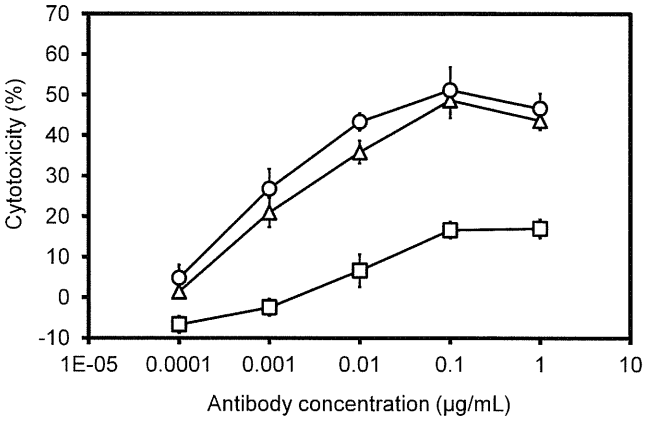

Fig. 2. ADCC of antibody Fc variants. ADCC of IgG1, afucosyl mAb, and asym-mAb23 was determined by percent lysis of DLD-1 cells expressing opsonized tumor antigen A at varying concentrations of antibody Fc variants to tumor antigen A, using PBMC as effector cells. Square, IgG1; triangle, afucosyl mAb; and circle, asym-mAb23. Mean ± S.D. of triplicate wells.

structure factors have been deposited at the Protein Data Bank (PDB) with the codes 3WN5.

3. Results and discussion

3.1. SPR analysis of FcγR binding affinity and ADCC

We optimized Fc variants asymmetrically to increase the binding affinity for both FcγRIIIa and FcγRIIa by utilizing the comprehensive mutagenesis in FcγR binding sites of the C_H2 domain, as we explained in our previous report (Mimoto et al., 2013). As a result, we obtained a variant, asym-mAb23, by introducing L234Y/L235Y/G236W/S239M/H268D/S298A/A327D substitutions into one heavy chain Fc region and D270E/K326D/A330K/K334E substitutions into the other heavy chain Fc region, which enhanced binding affinity for FcγRIIa by 67-fold and for FcγRIIIa by 1000-fold compared with wild-type mAb, as shown in Fig. 1. The kinetic parameters (k_a, k_d, and K_D) of each antibody are shown in supplementary Table 1 and representative sensorgrams are depicted in supplementary Fig. 1. The FcγRIIa binding affinity of asym-mAb23 was comparable with that of the most potent symmetrically engineered Fc variant with G236A/S239D/I332E (ADE) substitutions (Fig. 1). The FcγRIIIa binding affinity of asym-mAb23 was also comparable with that of the most potent symmetrically engineered Fc variant with S239D/A330L/I332E (DLE) substitutions (Fig. 1). Asym-mAb23 achieved the most potent binding to FcγRIIa and FcγRIIIa at the same time, which could not be achieved by symmetrically engineered Fc variants.

The ADCC activity of asym-mAb23 was compared with that of wild-type IgG1 and afucosyl mAb using human PBMC. Asym-mAb23 showed greater ADCC activity than IgG1 and slightly higher or comparable activity with afucosyl mAb (Fig. 2).

3.2. Overall structure of the asymmetrically engineered Fc variant in complex with FcγRIIIa

The 2.78 Å resolution crystal structure was determined for the complex of Fc (asym-mAb23) with human FcγRIIIa. In an asymmetric unit of the crystal, two 1:1 complexes of Fc (asym-mAb23) and FcγRIIIa, complex 1 (Fig. 3A) and complex 2 (Fig. 3B), were observed. In both of the complexes, Fc (asym-mAb23) binds to FcγRIIIa at the lower hinge region and C_H2 domains, as observed in the previously reported crystal structures of Fc and FcγR complexes (Ferrara et al., 2011; Sondermann et al., 2000; Radaev et al., 2001; Ramsland et al., 2011), one of which (PDB ID: 3SGJ) is shown in Fig. 3C. The rms difference of the whole main chain atoms between the two complexes in the asymmetric unit is slightly large, at 2.03 Å. However, the rms difference of the main chain atoms in the binding region consisting of domain 2 of FcγRIIIa and the C_H2 domains of the Fc (asym-mAb23) is 1.60 Å.

Theoretically, an asymmetrically engineered Fc variant is able to interact with FcγRs in two different orientations, since the Fc region recognizes the FcγR asymmetrically from each side of the region. However, in this crystal structure, Fc (asym-mAb23) has the same asymmetric binding orientation toward FcγRIIIa in each complex. The chain of Fc (asym-mAb23) with D270E/K326D/A330K/K334E substitutions binds to the side of FcγRIIIa that comprises W87, W110, and K158, and the other chain with L234Y/L235Y/G236W/S239M/H268D/S298A/A327D substitutions binds to the other side of FcγRIIIa that comprises K117, Y129, and H131. This result suggests that asym-mAb23 recognized FcγRIIIa or FcγRIIa only in a favorable manner.

Between the FcγRIIIa and Fc (IgG1) complex (PDB ID: 3SGJ) and complex 1 of the Fc (asym-mAb23) and FcγRIIIa in this crystal, rms difference of the main chain atoms in the binding region is 1.65 Å and between the FcγRIIIa and Fc (IgG1) complex and complex 2, that is 1.03 Å. This result indicates that the protein structure of complex 2 is more similar to the FcγRIIIa and Fc (IgG1) complex than complex 1 is. Most of the key interactions observed between Fc (IgG1) and FcγRIIIa are conserved. For example, P329 in the C_H2-A of complex 1 and complex 2 forms tight hydrophobic interactions with W87 and W110 of FcγRIIIa, and D265 in the C_H2-B of both of the complexes forms a potent electrostatic interaction with K117 of FcγRIIIa in a similar way to the reported FcγRIIIa and Fc (IgG1) complex structures.

The structure of the carbohydrate chains attached to N159 of FcγRIIIa is different between the complexes. In complex 1, the electron density of five branched sugar moieties of FcγRIIIa was observed, similar to that seen in the FcγRIIIa and Fc (IgG1) complex (Ferrara et al., 2011), and those sugar moieties are involved in the interaction with a carbohydrate chain of Fc (asym-mAb23). On the other hand, in complex 2, the electron density of only three sugar moieties was observed, and these are not involved in the interaction with Fc (asym-mAb23).

These differences observed in the two complexes in an asymmetric unit may suggest that Fc (asym-mAb23) could bind to

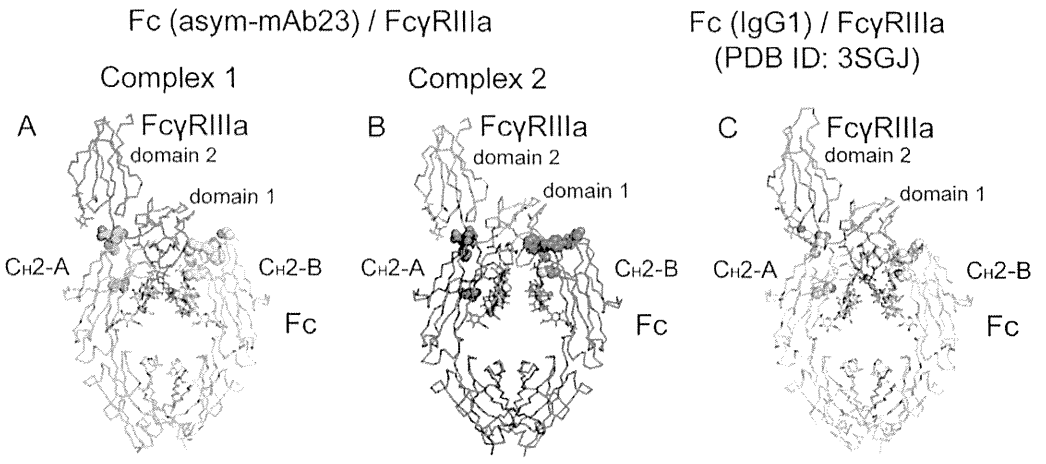

Fig. 3. The overall structure of Fc (asym-mAb23) and FcγRIIIa complexes in the asymmetric unit in comparison with a known Fc (IgG1) and FcγRIIIa complex. (A) The Cα trace of Fc (asym-mAb23) and FcγRIIIa complex 1. Complex 1 consists of two Fc fragments and FcγRIIIa. The Fc fragment with D270E/K326D/A330K/K334E substitutions is shown in green (Fc fragment A) and the other Fc fragment with L234Y/L235Y/G236W/S239M/H268D/S298A/A327D substitutions in cyan (Fc fragment B). FcγRIIIa is shown in magenta. (B) The Cα trace of Fc (asym-mAb23) and FcγRIIIa complex 2. Complex 2 consists of two Fc fragments and FcγRIIIa. Fc fragment A is shown in red and Fc fragment B in blue. FcγRIIIa is shown in orange. (C) The Cα trace of a known Fc (IgG1) and FcγRIIIa complex (PDB ID: 3SGJ). The complex consists of two Fc fragments and FcγRIIIa. Fc fragment A and B are corresponding to those of Fc (asym-mAb23) and FcγRIIIa complex. Both of the Fc fragments are shown in yellow and FcγRIIIa in gray. The substituted residues in Fc (asym-mAb23) and the corresponding residues in Fc (IgG1) are shown by spheres. The carbohydrate chains of the heavy chain Fc region and of FcγRIIIa are shown by sticks.

FcγRIIIa in several different manners, although the difference may also be influenced by the crystal packing environment.

3.3. Structural implication of the contribution of each substitution of asym-mAb23 to the improved FcγRIIIa binding

The interfaces between the C_H2-A of Fc (asym-mAb23) and FcγRIIIa in complexes 1 and 2 are depicted in Fig. 4. In the C_H2-A of Fc (asym-mAb23), four substitutions, D270E/K326D/A330K/K334E, are introduced. Structural superposition of the C_H2-A of FcγRIIIa and Fc (IgG1) complex (PDB ID: 3SGJ) with the C_H2-A of complex 1 and complex 2 results in 0.75 Å and 0.67 Å rms differences of the main chain atoms, respectively. These substitutions do not affect the main chain structure of the C_H2-A, but affect the side chain structures around the residues.

In the C_H2-A, all of the substituted residues are charged, which would improve long-range electrostatic interactions with FcγRIIIa. In both of the complexes in this crystal, D270E would optimize the electrostatic interaction with K111 of FcγRIIIa (Fig. 4A and B); K326D would change electrostatic repulsions with K19 of FcγRIIIa to electrostatic attractions (Fig. 4A and B); A330K would make a new electrostatic interaction with E163 of FcγRIIIa and enhance van der Waals contacts with I85 of FcγRIIIa (Fig. 4A and B). The conformation of these side chain residues and the distances of ion-pairs are slightly different between the two complexes. This might reflect the weakness of these long-range electrostatic interactions. The contribution of K334E to the enhancement of FcγRIIIa binding seems mediated by a different mechanism from those of other substitutions. K334E makes a hydrogen bond with the carbohydrate chain attached to N297 of the C_H2-A of complex 1 and complex 2 (Fig. 4C and D), which could result in changing and stabilizing the carbohydrate chain conformation. The carbohydrate chain of the heavy chain Fc region is known to be critical for the binding to FcγRs (Ferrara et al., 2011; Krapp et al., 2003), so modifying and stabilizing the carbohydrate chain conformation could contribute to enhancing the binding activity to FcγRs.

The interfaces between the C_H2-B of Fc (asym-mAb23) and FcγRIIIa in complex 1 and 2 are depicted in Fig. 5. The substitutions introduced into the C_H2-B domain of Fc (asym-mAb23), L234Y/L235Y/G236W/S239M/H268D/S298A/A327D, affect not only the side chain structures around the substituted residues, but also the main chain structure of the lower hinge region, loop 265–273, and loop 325–331. Structural superposition of the C_H2-B of complex 1 with the C_H2-B of FcγRIIIa and Fc (IgG1) complex (PDB ID: 3SGJ) results in 1.13 Å rms difference of the main chain atoms. The lower hinge and some of the loops show larger deviations; with regard to residues 235–237 in the lower hinge, loop 265–273, and loop 325–331, the largest rms differences of the main chain are observed at Y235, P271, and D327, respectively, and their values are 4.85 Å, 2.18 Å, and 3.91 Å, respectively. Similar lower hinge and loop deviations are observed in the C_H2-B of complex 2. Structural superposition of the C_H2-B of complex 2 in this crystal structure with the C_H2-B of FcγRIIIa and Fc (IgG1) complex (PDB ID: 3SGJ) results in 0.77 Å rms difference of the main chain atoms. On the other hand, with regard to residues 235–237 in the lower hinge, loop 265–273, and loop 325–331, the largest rms differences of the main chain are observed at the same residues as in the C_H2-B of complex 1 (Y235, P271, and D327, respectively) and their values are 3.00 Å, 2.59 Å, and 2.27 Å, respectively. Compared with the FcγRIIIa and Fc (IgG1) complex, the electron density of the lower hinge is not well observed, especially in the C_H2-B. In both of the complexes, the conformation of L234Y and the preceding residues are not defined.

Some structural differences are observed around L235Y and G236W between the C_H2-B of complex 1 and complex 2; the main difference being that the two residues are interchanged between the two complexes and adopt conformations that are both different from that of the FcγRIIIa and Fc (IgG1) complex. In complex 1, W236 is involved in a hydrophobic core of the C_H2-B domain with P238, L328, V323, and I332 of the same domain, which can shift loop 325–331 considerably from the corresponding loop observed in the Fc (IgG1) and FcγRIIIa complex. L235Y of C_H2-B in complex 1 forms a van der Walls contact with K117 and edge-to-face interactions with H116 and H132 of FcγRIIIa (Fig. 5A). On the other hand, in the C_H2-B domain of complex 2, W236 is not involved in the hydrophobic core of the same domain, as is observed in the C_H2-B of complex 1. Instead, it forms a stacking interaction with H116 of FcγRIIIa, with L235Y of C_H2 making contact with L328 and P329 in the same domain (Fig. 5B). In complex 1, H268D would make a new electrostatic interaction with K128 of FcγRIIIa. Moreover,

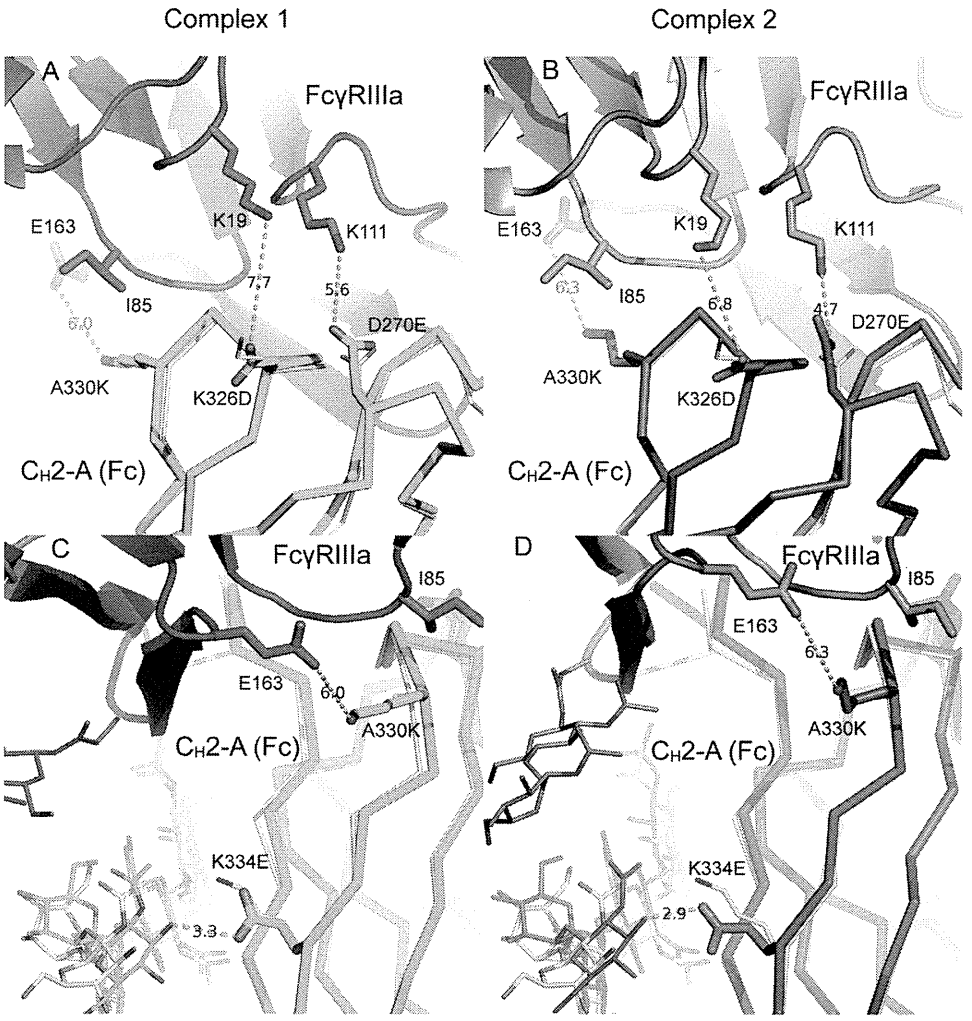

Fig. 4. The binding interfaces between the C_H2-A of Fc (asym-mAb23) and FcγRIIIa in complexes 1 and 2. The binding interfaces between the C_H2-A (shown in green) of Fc (asym-mAb23) and FcγRIIIa (shown in magenta) in complex 1 and the corresponding binding interfaces between the C_H2-A (shown in red) of Fc (asym-mAb23) and FcγRIIIa (shown in orange) in complex 2 are depicted in (A) and (B), respectively. The binding interfaces of another angle between the C_H2-B of Fc (asym-mAb23) and FcγRIIIa in complex 1 and 2 are depicted in (C) and (D), respectively. The corresponding C_H2 domain structure of the Fc (IgG1) (PDB ID: 3SGJ) (shown in yellow) is superimposed on the C_H2-A domain of Fc (asym-mAb23).

H268D may change the side chain conformation of neighboring residues E269 and E294 in C_H2-B of complex 1 and thus may contribute to optimizing the electrostatic interactions of those residues with K128 and K125 of FcγRIIIa, respectively (Fig. 5A). On the other hand, in complex 2, the conformations of K125 and K128 of FcγRIIIa are not completely defined because their electron density is poor (Fig. 5B), and this suggests that the long-range electrostatic interactions related to H268D might be weaker than others. As shown in Fig. 5A and B, in complex 1 and complex 2, S298A reduces the size of the side chain of the residue, which might result in optimizing a van der Waals interaction with FcγRIIIa to achieve closer binding in the whole binding surface of the C_H2-B in the Fc region. S239M makes new van der Waals contacts with K117 of FcγRIIIa and with the carbohydrate chain attached to N297 of the C_H2-B of complex 1 and complex 2 (Fig. 5C and D). This mutation might also contribute to stabilizing the carbohydrate chain conformation and enhancing the binding activity for FcγRs. The direct contribution of A327D to the improved binding affinity to FcγRIIIa is not obvious from the structural analysis, because even the nearest possible partner residues in FcγRIIIa, K117 and K128, are too far (approximately 14 Å) to form effective electrostatic interactions in either of the complexes. In the Fc (IgG1) and FcγRIIIa complex, A327 is located close enough to D270, so A327D might introduce an electrostatic repulsion with D270 to trigger the conformational change of loop 265–273 and loop 324–331. This would be the reason why the side chain of D270 of Fc (asym-mAb23) forms a hydrogen bond with the side chain of H131 of FcγRIIIa, which was not observed in Fc (IgG1) bound to FcγRIIIa. As a result, this substitution may contribute to the improvement of binding activity to FcγRIIIa.

As described above, the X-ray crystal structure suggests that the contribution of each substitution to the binding affinity is moderate. This is indicated by the distant electrostatic interactions (4–9 Å) observed in the structure and is also suggested by the fact that two types of binding mode were observed in some parts of the interface between Fc (asym-mAb23) and FcγRIIIa. Some of the substitutions seem to contribute to the binding enhancement indirectly by stabilizing the carbohydrate chains of the heavy chain Fc region or changing the loop conformation. Nevertheless, asym-mAb23 showed approximately 1000-fold enhanced binding affinity for FcγRIIIa. This would be achieved by the cumulative effect of these weak direct effects and the indirect effects caused by the stabilization of the carbohydrate chain conformation and the change of loop conformation.

A previous report suggested the difficulty of maintaining the high stability and improving the binding affinity for FcγRs at the same time by protein-engineering of Fc region (Oganesyan et al.,

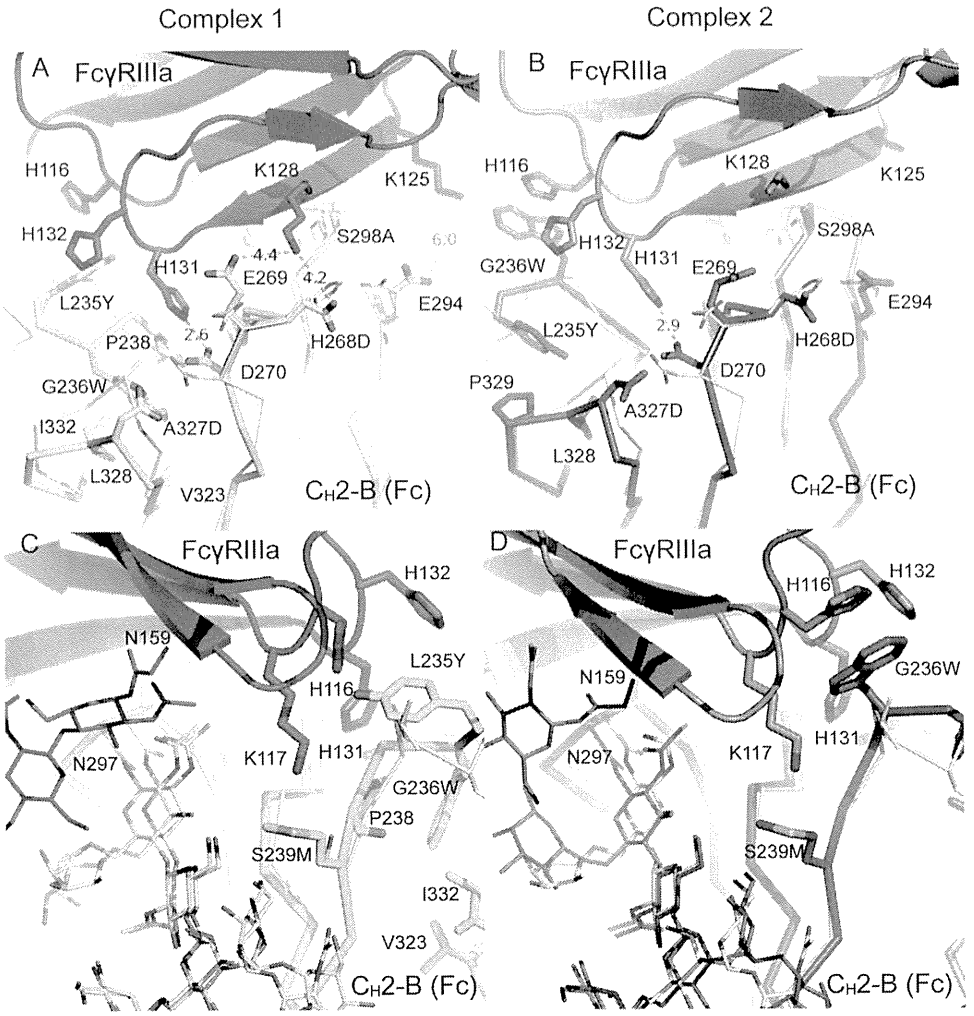

Fig. 5. The binding interfaces between the C_H2-B of Fc (asym-mAb23) and FcγRIIIa in complexes 1 and 2. The binding interfaces between the C_H2-B (shown in cyan) of Fc (asym-mAb23) and FcγRIIIa (shown in magenta) in complex 1 and the corresponding binding interfaces between the C_H2-B (shown in blue) of Fc (asym-mAb23) and FcγRIIIa (shown in orange) in complex 2 are depicted in (A) and (B), respectively. The binding interfaces of another angle between the C_H2-B of Fc (asym-mAb23) and FcγRIIIa in complex 1 and 2 are depicted in (C) and (D), respectively. The corresponding C_H2 domain structure of the Fc (IgG1) (PDB ID: 3SGJ) (shown in yellow) is superimposed on the C_H2-B domain of Fc (asym-mAb23).

2008). However, asymmetric Fc engineering can minimize the number of total substitutions in the Fc region, as we discussed in the previous report (Mimoto et al., 2013). In other words, asymmetric Fc engineering enables us to utilize a large number of substitutions and to exploit their contributions, even those conferring weak enhancement.

4. Conclusion

This is the first report describing the crystal structure of an asymmetrically engineered Fc variant in complex with FcγRIIIa. The structural analysis suggested that the asymmetrically introduced substitutions fine-tuned the interaction in each interface between the C_H2 domain and FcγRIIIa. Thus, the application of asymmetric Fc engineering would enable us to optimize the interaction in each interface independently and thus design Fc variants with a variety of FcγRs binding profiles more precisely. This crystal structure could be utilized when we design a more potent asymmetric Fc variant.

Acknowledgments

We thank our colleagues at Chugai Research Institute for Medical Science, Inc. and Chugai Pharmaceutical Co., Ltd., M. Fujii, Y. Nakata, A. Maeno, and S. Masujima for antibody generation; M. Saito for carrying out SPR analysis; and A. Sakamoto, M. Okamoto, and M. Endo for carrying out preparation of FcγRs. This work was fully supported by Chugai Pharmaceutical Co., Ltd.

Appendix A. Supplementary data

Supplementary data associated with this article can be found, in the online version, at http://dx.doi.org/10.1016/j.molimm.2013.11.017.

References

DeLano, W.L., 2002. The PyMOL Molecular Graphics System. Schrödinger, LLC, Palo Alto, CA.
Emsley, P., et al., 2010. Features and development of Coot. Acta Crystallogr. 66D, 486–501.
Evans, P., 2006. Scaling and assessment of data quality. Acta Crystallogr. 62D, 72–82.
Ferrara, C., et al., 2011. Unique carbohydrate–carbohydrate interactions are required for high affinity binding between FcgammaRIII and antibodies lacking core fucose. Proc. Natl. Acad. Sci. U. S. A. 108, 12669–12674.
Green, S.K., et al., 2002. Disruption of cell–cell adhesion enhances antibody-dependent cellular cytotoxicity: implications for antibody-based therapeutics of cancer. Cancer Res. 62, 6891–6900.

Jung, S.T., et al., 2010. Aglycosylated IgG variants expressed in bacteria that selectively bind FcgammaRI potentiate tumor cell killing by monocyte-dendritic cells. Proc. Natl. Acad. Sci. U. S. A. 107, 604–609.
Kabsch, W., 1976. A solution for the best rotation to relate two sets of vectors. Acta Crystallogr. A 32, 922–923.
Kabsch, W., 2010. XDS. Acta Crystallogr. 66D, 125–132.
Klein, C., et al., 2012. Progress in overcoming the chain association issue in bispecific heterodimeric IgG antibodies. MAbs 4, 653–663.
Krapp, S., et al., 2003. Structural analysis of human IgG-Fc glycoforms reveals a correlation between glycosylation and structural integrity. J. Mol. Biol. 325, 979–989.
Lazar, G.A., et al., 2006. Engineered antibody Fc variants with enhanced effector function. Proc. Natl. Acad. Sci. U. S. A. 103, 4005–4010.
McCoy, A.J., et al., 2007. Phaser crystallographic software. J. Appl. Crystallogr. 40, 658–674.
Mimoto, F., et al., 2013. Novel asymmetrically engineered antibody Fc variant with superior FcγR binding affinity and specificity compared with afucosylated Fc variant. MAbs 5, 229–236.
Murshudov, G.N., et al., 2011. REFMAC5 for the refinement of macromolecular crystal structures. Acta Crystallogr. 67D, 355–367.
Oganesyan, V., et al., 2008. Structural characterization of a mutated, ADCC-enhanced human Fc fragment. Mol. Immunol. 45, 1872–1882.
Radaev, S., et al., 2001. The structure of a human type III Fcgamma receptor in complex with Fc. J. Biol. Chem. 276, 16469–16477.
Ramsland, P.A., et al., 2011. Structural basis for Fc gammaRIIa recognition of human IgG and formation of inflammatory signaling complexes. J. Immunol. 187, 3208–3217.
Richards, J.O., et al., 2008. Optimization of antibody binding to FcgammaRIIa enhances macrophage phagocytosis of tumor cells. Mol. Cancer Ther. 7, 2517–2527.
Sazinsky, S.L., et al., 2008. Aglycosylated immunoglobulin G1 variants productively engage activating Fc receptors. Proc. Natl. Acad. Sci. U. S. A. 105, 20167–20172.
Scott, A.M., et al., 2012. Monoclonal antibodies in cancer therapy. Cancer Immun. 12, 14.
Shields, R.L., et al., 2002. Lack of fucose on human IgG1 N-linked oligosaccharide improves binding to human Fcgamma RIII and antibody-dependent cellular toxicity. J. Biol. Chem. 277, 26733–26740.
Shinkawa, T., et al., 2003. The absence of fucose but not the presence of galactose or bisecting N-acetylglucosamine of human IgG1 complex-type oligosaccharides shows the critical role of enhancing antibody-dependent cellular cytotoxicity. J. Biol. Chem. 278, 3466–3473.
Sondermann, P., et al., 2000. The 3.2-A crystal structure of the human IgG1 Fc fragment-FcγRIII complex. Nature 406, 267–273.
Stavenhagen, J.B., et al., 2007. Fc optimization of therapeutic antibodies enhances their ability to kill tumor cells in vitro and controls tumor expansion in vivo via low-affinity activating Fcgamma receptors. Cancer Res. 67, 8882–8890.
Winter, G., 2010. xia2: an expert system for macromolecular crystallography data reduction. J. Appl. Crystallogr. 43, 186–190.